15ÈMES JOURNÉES DE L'HYDRODYNAMIQUE
22 - 24 novembre 2016 - Brest

# PRESENTATION D'UNE CAMPAGNE EXPERIMENTALE POUR MESURER LES PERFORMANCES ET LES EFFETS D'UN KITE DE 50 MÈTRES CARRÉS INSTALLÉ SUR UN CHALUTIER DE 13 MÈTRES

*PRESENTATION OF AN EXPERIMENTAL CAMPAIGN FOR MEASURING PERFORMANCES AND EFFECTS OF A 50-SQUARE-METER KITE SET-UP ON A 13-METER TRAWLER*

**Morgan Behrel [(1)*], Kostia Roncin [(1)], Damien Grelon [(2)], Fréderic Montel [(1)], Alain Nême [(1)], Jean-Baptiste Leroux [(1)], Christian Jochum [(1)], Yves Parlier [(3)]**
[(1)] ENSTA Bretagne, FRE CNRS 3744, IRDL, F – 29200 Brest, France
[(2)] MERINOV, Grande Rivière, Québec, Canada
[(3)] BEYOND THE SEA, 1010 avenue de l'Europe, 33260 La Teste de Buch, France
* Contact: morgan.behrel@ensta-bretagne.org

## Résumé

Cet article décrit une campagne de mesure en mer réalisée sur un chalutier de 13 mètres équipé d'un kite de 50 mètres carrés. Cette campagne s'est déroulée à Grande Rivière, Gaspésie, province de Québec, Canada, en octobre 2015. Le but était d'évaluer les performances du navire lorsque le kite est déployé. Pour cela, en plus des dispositifs de contrôle du kite, un ensemble de capteurs a été installé. Ainsi de nombreuses données ont été enregistrées comme la vitesse et le cap du navire, les efforts générés par le kite, la consommation du moteur, les mouvements du bateau, le couple et la vitesse de rotation de l'arbre d'hélice, l'angle du gouvernail ou la vitesse du vent.

Au cours de la campagne, des phases rectilignes avec le kite fonctionnant en vol statique ont été effectuées, avec environ 12 nœuds de vent réel. Le post-traitement des données qui est présenté permet d'estimer la finesse du kite en vol statique ainsi que son coefficient de portance. La valeur de la finesse obtenue est autour de 6, ce qui est cohérent avec d'autres résultats expérimentaux publiés.

## Summary

This paper describes an onboard measurement campaign held in Grande-Rivière, Gaspésie, province of Québec, Canada, in October 2015, involving a 13-meter trawler equipped with a 50-square-meter kite. The aim of the campaign was the assessment of the boat performances when kite is used. To achieve this purpose, in addition to the kite control system, a set of sensors has been installed. Thus data were recorded, as boat velocity, force generated by kite, fuel consumption, boat attitude, torque and rotational speed of propeller shaft, rudder angle and wind velocity.

During the trials, runs with kite in static flight were done, with around 12 knots of true wind speed. The data post processing is presented in this paper, and allows to estimate a lift to drag ratio around 6 of the kite and the tethers. This is consistent with other experimental data published.

**Nomenclature**

| | |
|---|---|
| $AR$ | Aspect Ratio of the kite |
| $Fi$ | Component of the kite force along the i-axis into the reference frame subscripted |
| $L/D$ | Lift to drag ratio of the kite |
| $V_a$ | Kite apparent wind speed |
| $V_{WR}$ | Relative Wind speed at kite altitude |
| $\underline{V}_{WR}$ | Relative Wind velocity vector at kite altitude |
| $\underline{V}_{WT}$ | True Wind velocity vector |
| $\beta_{\mathrm{WR}}$ | Relative wind angle at kite altitude (relative to ship axis) |
| $\rho_a$ | Air density during experiments |
| $\rho_w$ | Water density |
| $\psi$ | Heading angle of the ship |

**Reference Frames**

$\Re_0$ is the earth fixed coordinate system, using the North East Down (NED) convention.

$\Re_S$ is the ship coordinate axis system, rigidly fixed to the ship. It is defined with the Z-axis pointing down, the X-axis pointing forward, and the Y-axis pointing to starboard. The origin of reference frame is at mid-ship, in the intersection between the center plane of the boat and the water plane.

$\Re_\psi$ is the heading coordinate axis system. It is the result of a rotation about axis $Z_0$ of heading angle $\psi$ applied to frame $\Re_0$.

$\Re_{WR}$is the relative wind coordinate axis system at kite altitude. It is the result of a rotation about axis $Z_0$ of angle ($\beta_{\mathrm{WR}}$ - $\pi$) applied to frame $\Re_0$.

$\Re_K$ is the body reference frame attached to the kite, assumed as a rigid body.

## 1. Introduction

The use of kite to extract energy from wind is not a new idea, as it can be seen in Lloyd [1]. However, the current growing shortage of fossil resources and the emergence of new ecological regulations force us to reconsider more renewable options, and the use of kite is one of them. The various ways to extract energy with kites have been properly summarize by Fagiano and Milanese in [2], and Cherubini et al. [3] give a good oversight of possible technologies. The current research project, undertaken by the company **beyond the sea®**, and managed in partnership with ENSTA Bretagne, aims to develop kite as auxiliary propulsion system for ships.

For this purpose, numerical models have been developed at ENSTA Bretagne, and so forces generated by kite and associated fuel savings can be predicted [4]. Other models are also under development, in particular a parametrical maneuvering model to simulate the interaction between the kite and the ship[5]. All these tools need to be validated, and experimental comparison is one of the best ways to do it. In this context, a sea trial and measurement campaign has been set up in partnership with a Canadian fishing vessel and the Merinov institute. This campaign held in Grande-Rivière, Gaspésie, Province of Québec, Canada in October 2015. The fishing vessel was a 13-meter trawler usually used for fishing shrimps on the Gulf of St. Lawrence. All specifications will be given in the first part. A set of winches and sensors has been installed on board, to control the 50-square-meter kite, and measure the induced effects. All the experimental set up will be describe in Section 3.

First, mmaneuverability tests were carried out without kite, following as far as possible the ITTC guidelines [6]. This aimed to get data to benchmark a maneuvering model based on work done by Yoshimura and Masumoto [7]. Explanation on this model and validation method using data acquired with the presented experimental set-up are detailed by Bigi in [5]. Secondly, runs with kite in static flight were carried out. Logged data were used to compute lift to drag ratio and lift coefficient

of the kite, using a method presented in Section 4. This method is specifically adapted to the available data. Indeed, due to a lack of some information on kite orientation during flight and on wind along the altitude, strong assumptions and estimations have to be done, leading to results which must be interpreted with caution. However, the obtained lift to drag ratios and lift coefficients make sense with other experimental works like Dadd one [8].

## 2. General presentation of experimental set up

### 2.1. Characteristics of the kite

The kite used during trials had an area of 50 square-meters (34 square-meters of projected area), with an inflatable leading edge, and 9 inflatable battens (see Fig. 1). With this architecture, the kite has his own shape without any aerodynamic load, so launching and recovering procedure are easier. The mass of the deflated kite with bridles is 21 kg.

Four 60-meter-tethers link the kite to the boat. The two main ones, so-called front tethers, are linked to the bridle system attached on the leading edge, and resume about 80% of forces generated by kite. Their lengths are constant. The 20% remaining are taken by the back tethers, which are linked to another bridle system attached on the battens. Back tether are used to control kite flight, and for this purpose their lengths can vary. The attachment point of the tethers was located just ahead the forward bulkhead of the wheelhouse, as it can be seen in Fig. 2. The mass of the 4 tethers is 2 kg.


Fig. 1: Kite used during measurement. C-shape with inflatable leading edge and battens, 50m², 23 kg (deflated, with bridles and tethers).

For launching and recovering procedures, all tethers are wound on the same winch. For control purpose, each back tethers goes through a specific pulley system, whose length is adjustable using electric winches. Each one is powered with 24 V DC, and can deliver 700W of nominal power. Optical encoders are fixed on each motor to ensure a feedback to the control system.

The latter is running Windows 7, and the software controlling motors operates in LabVIEW (National Instruments). This one allows two mode of control: automatic and manual. The automatic one maintains the kite on a specified stationary position, using a small Inertial Measurement Unit (IMU) attached on the kite to get a feedback on kite position and orientation. The IMU uses a wireless connection to send data to the control system. This autopilot can only ensure static flight, which means the kite can only fly on the wind window edge. It has been developed by engineers of **beyond the sea®**, but this paper does not aim to give more details about it. The manual mode allows the operator to control directly the motor, using two joysticks. The first joystick acts on the differential length between the two back tethers, and so on the direction of the kite. The second joystick is used to trim simultaneously the length of the two back tethers, that means adjust the global angle of incidence of the kite. The kite control system is fully independent from the data acquisition system that will be described later.

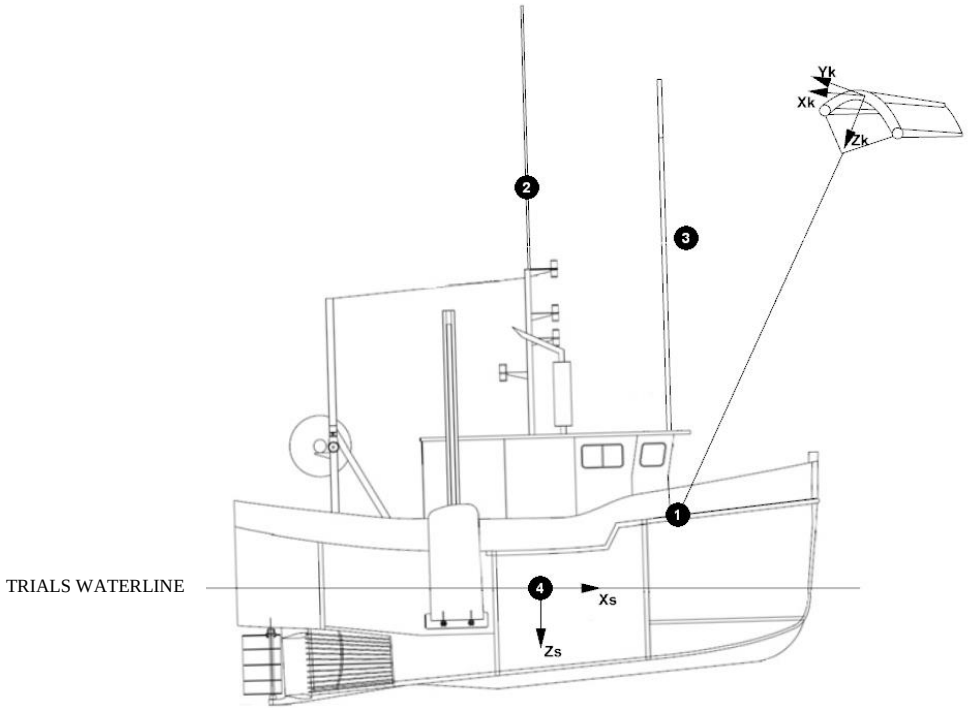


Fig. 2: Side view of the Steven Paul with the waterline as it was during trials. Marker 1 denotes the kite attachment point as well as the position of the 3D load cell described part 3.3. Marker 2 shows the position of the anemometer described part 3.4. Marker 3 notes the launching mast used for launching and recovering procedures. Marker 4 shows the mid-ship of the boat and the origin of the $\Re_S$ reference frame. Kite size and tether length are not true to scale.

### 2.2. Characteristics of the vessel

The trials were conducted on a 13-meter fishing vessel, called Steven Paul, used to fish shrimps with trawl on Saint Laurence gulf during summer season. General information and dimensions are given in Table I; a side view plan is given in Fig. 2 and a picture in Fig. 3. The Steven Paul, like the majority of the fishing vessels of the area, is equipped with lateral stabilizers to reduce roll motion, and so, improve working comfort of the crew. Internal structure modifications have been carried out to allow the use of a towing kite, especially by reinforcing the foredeck on which kite tethers were attached.

Table I: General characteristics of the fishing vessel Steven Paul

| | | |
|---|---|---|
| Length Overall | 13.39 | m |
| Length of waterline (trials loading conditions) | 12.89 | m |
| Length between perpendiculars | 12.28 | m |
| Beam of the hull | 5.61 | m |
| Displacement (trials loading conditions) | 64 | T |
| Displacement (full load) | 90 | T |
| Maximum Draft (trials loading conditions) | 2.66 | m |
| Draft (full load) | 3.23 | m |
| Motorization | Caterpillar 3408 - 480hp | - |
| Propulsion | Ducted Propeller | - |
| Crew for fishing operations | Captain with 2 seamen | - |

Fig. 3: Picture of the Steven Paul.

Fig. 4: Onboard picture of the kite in static flight during one of the starboard run.

A Caterpillar 480 horse power engine ensures the propulsion of the vessel (model Marine 3408). At full power (during trawling operation or maximum transit speed), the fuel consumption is about 80 liters per hour. A reduction gear, with a transmission ratio of 1:4.48 transfers power to the propeller (Fig. 5). The latter is a 4 blades ducted propeller, with diameter of 1.26 meter. A grid is protecting propeller from unidentified floating objects or from the fishing ropes in case of problem during trawling operation. The characteristics of the propeller are given in Table II.

The rudder is a flat plate (Fig. 5), 1.45 meter high, for 0.84 meter chord, driven by a hydraulic actuator.

Table II: Propeller characteristics of the fishing vessel Steven Paul

| | | |
|---|---|---|
| Propeller Diameter | 1.26 | m |
| Number of blades | 4 | - |
| Pitch Ratio | 1.015 | - |
| Blade Area Ratio | 0.55 | - |

Fig. 5:Pictures of the Steven Paul propeller and rudder.

### 2.3. Data acquisition system

The whole data acquisition system is based on a National Instruments CompactRIO platform. It consists of 3 main parts: a set of I/O modules depending on sensor technology, a Field-Programmable Gate Array (FPGA, NI CRIO-9114) and a Real-Time processor (NI CRIO-9024). All I/O modules are connected to the FPGA, and the very accurate clock of the FPGA ensures a good

synchronization between the channels, and precise acquisition frequencies. The Real-Time processor logs all data coming from sensors through the FPGA on a non-volatile memory. Table III gives the details of I/O modules which have been used for this campaign. All acquisition programs have been developed with LabVIEW.

Table III: Summary of National Instrument I/O module used for data acquisition

| Module | Description | Total number of channels |
|---|---|---|
| 2 x NI 9870 | Serial Port | 8 |
| 1 x NI 9411 | Digital Input | 6 |
| 2 x NI 9237 | Bridge Analog Input | 8 |

Raw data were all stored in a single file, using a National Instruments proprietary format (TDMS file). These files were then converted into MATLAB® format files, and all calibration procedures and data processing were done using this software.

## 3. Sensors

### 3.1. Kinematics of the vessel

To measure motions and velocities of the boat, an IMU coupled with a GPS was set up (Xsens MTi-G-700). This Unit includes a microprocessor able to realize data fusion, based on an extended Kalman filter providing roll and pitch information. Manufacturer ensures dynamic error for roll and pitch under 1° with a 1σ RMS error of 0.1°. The acquisition frequencies of the Xsens were 50Hz for inertial sensors (gyroscope and accelerometer), 20 Hz for roll and pitch, and 5 Hz for all data regarding GPS technology (position and velocity). The Xsens was directly linked to a serial port of the CompactRIO. It was fixed in the wheelhouse, just behind the forward bulkhead, a few centimeters behind the attachment point of the kite, located ahead this bulkhead.

To avoid complex and unreliable calibration procedure of magnetometers, it has been decided to use an existing onboard sensor to get yaw information, based on dual antenna GPS, instead of yaw information provided by the magnetometers of the Xsens. The sensor was a Si-Tex Vector Pro, with 1σ RMS error under 0.3°. This sensor, providing the true heading of the boat regardless the boat velocity, is used by the onboard autopilot. Therefore, a serial link was done between the autopilot and the CompactRIO to recover this information. The maximum update rate of the Si-Tex Vector Pro is up to 20 Hz, according to the manufacturer. However, because the information goes through the autopilot before reaching the data acquisition system, the final update rate was 1Hz. This could not be changed during the campaign.

### 3.2. Engine and rudder system

A double flowmeter had been installed previously on the engine, to measure the fuel feed and fuel return, and so provide fuel consumption (Maretron M2RSP-2R-E8). This sensor is connected to the on board NMEA 2000 network. A conversion device on the NMEA2000 network provides a serial output with NMEA183 protocol. This output was connected to another serial port of the CompactRIO, and so the fuel flow was logged at 1Hz.

A device measuring the torque on the propeller shaft, developed by the company UpDaq, had also been installed previously on board. A strain gauge had been stuck on the shaft and is linked to an amplifier, sending data wirelessly to a receiver in the wheelhouse. The latter was connected to the acquisition system through a serial link. The torque on the shaft was logged at 20 Hz.

The measurement of rotational speed of the shaft propeller was carried out thank to a binary sensor, going from 0 V to 5 V each time the shaft completes a revolution. The sensor was directly linked to the Digital Input module (NI 9411) of the CompactRIO system.

A rudder angle sensor was part of the autopilot system to provide feedback. This information had been retrieved using the existing serial link presented part 3.1, with a resolution of 1°, and a frequency of 1 Hz.

### 3.3. Kite

To get forces on tethers, load cells had been used during trials. A three dimension load cell (Michigan Scientific TR3D-4K) had been rigidly fixed on the foredeck, just in front the forward bulkhead of the wheelhouse. The location in $\Re_S$ reference frame is (3.1 m, 0 m, -1.7 m). This load cell has a full scale load of 17,800 N for each axis, with a safe overload of 300%. The selection process of the load cell range was done using simulation tools developed by Leloup et al. [4]. During measurement phases, i.e. excluding launching and recovering procedures, the front tethers of the kite were directly connected to this load cell, without any idler pulleys. So, this sensor provided information of force vector generated by the kite, expressed into the load cell axis system in a first time, and into the boat axis system after post processing (the position and orientation of the load cell implantation had been carefully measured). Knowing the length of tethers, and considering tethers are straight, the position of the kite in the wind window can be recovered. The non-linearity error specified by manufacturer is under 0.5% of full scale, and hysteresis and repeatability errors are under 0.05% of full scale each. It was not possible on the boat to carry out a complete calibration of measurement chain, so sensibilities provided by manufacturer had been used.

Measurement of forces in back tethers was different due to the variable length of these tethers to ensure kite control. Two one dimension load cell (Futek LCM200) were installed into the pulleys system, and each one measured twice the load passing through each back tether. These load cells have a full scale load of 4,500 N, with a specified non-linearity error under 0.5% of full scale, a hysteresis error under 0.5% of full scale and repeatability error under 0.1% of full scale. Here again, full calibration procedure was difficult to carry out onboard, so sensibilities given on calibration certificate of each load cell has been used. The fact that measurement of back tether forces were done into a pulley circuit adds incertitude in measurement. The used pulleys were high-class ones with ball bearing design (Harken Carbo 57 mm), so it is sensible to expect limited effects, although no test in laboratory was carried out.

Each load cells and each axis of the 3D load cell were connected to one of the bridge analogical input of the CompactRIO system. The frequency of acquisition of all channels was 1 kHz.

### 3.4. Wind

Measurement of relative wind was done using an ultrasonic anemometer (LCJ Capteurs CV7) fixed at 9.01 m from the water line, and 0.3 m aft the mid-ship. The update rate of the sensor is 2 Hz, with a direction resolution of 1° and wind module resolution of 0.05 m/s. The sensor was linked to one of the serial port of the CompactRIO platform, using NMEA183 protocol.

The roll and pitch motion of the boat were small (maximum ±1°), with averaged periods of 2.9 s for pitch and 10 s for roll. These motions have induced a maximum velocity at the anemometer level of 0.2 m/s (3% of the averaged wind measured), and it has been decided to neglect these effects.

## 4. Post-processing of kite flight data

During the campaign, due to availability issues with the boat and inoperable weather, only one day of exploitable measurements was able to be achieved. During this day, runs with kite in static flight have been done, with about 12 knots of true wind speed. The aim of the following part is to process data to retrieve lift to drag ratio of the system {kite + tethers}. However, to compute the lift to drag ratio, the wind direction at the altitude of the kite needs to be known since it directly affects the

orientation of the wind window, and the associated reference frame $\Re_{WR}$. As it will be shown in Eq. (4) all the data must be expressed in $\Re_{WR}$. In the same way, to compute the lift coefficient, the wind intensity at the kite altitude needs to be known. Unfortunately, there was no reliable mean to measure it. Indeed only the relative wind over the boat, at 9 m over the sea, is measured (see Fig. 2). The true wind at the same location can be easily retrieved using the ship speed and heading information (see Eq. (1)), but the true wind at other altitude can only be estimated. Indeed, altitude impacts true wind both in strength and direction. With no possibility of getting accurate modelling of the twist of the flow along the altitude, it has been decided to neglect the effect of twist, and only take account the 2D shear stress distribution calculated using the Eq. (2), from the ITTC 2014 recommendations [9]. Equations (1) to (3) present the process to go from relative wind velocity and boat velocity measurement to relative wind velocity for any altitude *z*.

$$\underline{V}_{WT}(Z_0) = \underline{V}_{WR}(Z_0) + \underline{V}_S \tag{1}$$

$$\underline{V}_{WT}(z) = \left(\frac{z}{Z_0}\right)^{1/7} \underline{V}_{WT}(Z_0) \tag{2}$$

$$\underline{V}_{WR}(z) = \underline{V}_{WT}(z) - \underline{V}_S \tag{3}$$

Where $Z_0$ is the altitude measurement (m) and $z$ is the altitude above sea level (m). Rigorously, $\underline{V}_S$ has no reason to be permanently contained in the $(X_0, Y_0)$ plane. Indeed, boat motions induced a vertical velocity. However, considering the low level of boat motions during trials (lower than ±1°), the vertical component of the ship velocity is under 2% of the ship velocity magnitude. Hence, vertical speed of the ship has been neglected, and so $\underline{V}_S$ and $\underline{V}_{WR}$ are assumed to be contained in the $(X_0, Y_0)$. With the relative wind vector defined for any altitude, we can create a new axis system based on it. The Relative Wind reference frame is defined with the X-axis along the relative wind vector at the kite altitude, the Z-axis vertical pointing down and the Y-axis completing the coordinate system to create a direct one. This reference frame is noted with the subscript WR.

Because kite position measurement was done through a 3D load cell rigidly attached to the boat, boat motions affects kite position measurement. This is visible in Fig. 6 where elevation angle θ of the kite, resulting from the basic transformation of Cartesian position coordinates of the kite into spherical ones, according to boat axis system, evolves in line with the pitch of the boat. To remove these effects, position coordinates of the kite have been expressed into the $\Re_{\psi}$ axis system, independent from the boat pitch and roll motion. The transformation matrix is created from the first two Euler angles (roll and pitch) provided by the inertial measurement unit Xsens, according to Xsens User Manual [10]. Result of the transformation is given in Fig. 6, showing a few seconds of a starboard run with kite in static flight.

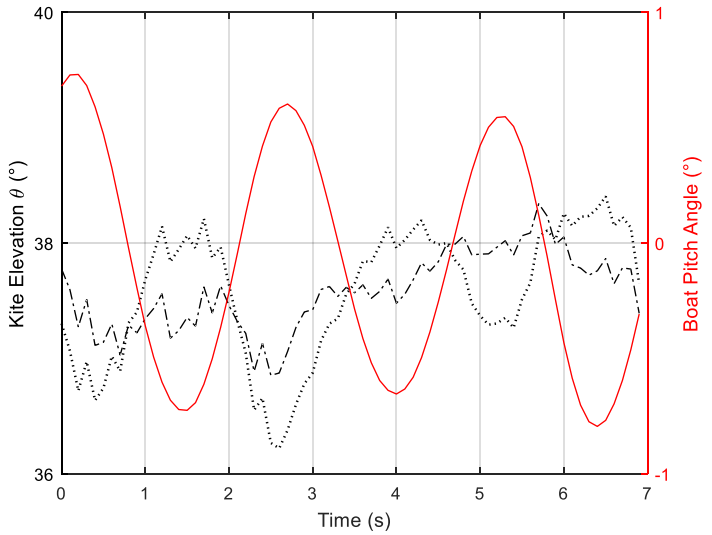


Fig. 6: Influence of pitch angle of the boat (solid red line) on kite position measurement. The dotted line is the expression of kite elevation angle in $\Re_S$, and the dash-dotted in $\Re_\psi$, during one of the runs with kite in static flight.

To process the lift to drag ratio and lift coefficient, the apparent wind on the kite needs to be known. This one is the vectorial difference between the relative wind and the kite velocity in the $\Re_\psi$ reference frame. For the specific case of static flight, with the ship moving a constant velocity, the kite velocity is theoretically zero in $\Re_\psi$. However kite in static flight undergoes small but permanent displacement around a middle position, but these displacements are mainly sideslip motion. With the used experimental set up, the yaw orientation of the kite was not measured, so the kite velocity vector cannot be known in the $\Re_K$ reference frame. To deal with this issue, it has been decided to consider the kite in perfect static flight at all times, i.e. the kite velocity in the $\Re_\psi$ reference frame is taken equal to 0. In other words, the kite is considered as continuously located on the wind window edge as defined by Leloup et al. [4], and the apparent wind vector is equal to the relative wind vector and is included in the symmetry plane of the kite assumed as a rigid body.

### 4.1. Lift to drag ratio estimation

From there, it becomes easy to compute lift to drag ratio by expressing kite forces in the $\Re_{WR}$ reference frame. Indeed, the component of the force along XWR-axis is the total drag, and the projection into the ($Y_{WR}$, $Z_{WR}$) plane is the lift. The component of force along the $Z_{WR}$-axis is the sum of the vertical aerodynamic force generated by kite and the weight $P$ of the kite and tethers (equals to 226 N). The latter is then subtracted to the vertical component of force to get only aerodynamic force. Finally the lift to drag ratio is achieved by processing the following equation:

$$L/D = \frac{\sqrt{Fy_{WR}{}^2 + (Fz_{WR} - P)^2}}{Fx_{WR}} \tag{4}$$

### 4.2. Lift Coefficient Estimation

The previous part has shown the identification of lift and drag component of kite force, from the measured force expressed in the relative wind axis system. From there, and with the same assumptions, lift coefficient can be processed using Eq. (5).

$$C_L = \frac{L}{\frac{1}{2} \cdot \rho_a \cdot A_k \cdot {V_a}^2} = \frac{\sqrt{{Fy_{WR}}^2 + (Fz_{WR} - P)^2}}{\frac{1}{2} \cdot \rho_a \cdot A_k \cdot {V_{WR}}^2} \quad (5)$$

$A_k$ is the projected kite area (34 $m^2$), $\rho_a$ is the density of the air, estimated to 1.22 $kg \cdot m^{-3}$ during the measurement day (air temperature 15°C, atmospheric pressure 1012 hPa, relative humidity 70%), $V_a$ is the kite apparent wind speed, equal to the relative wind speed $V_{RW}$ in case of static flight.

## 5. Results

The Eq. (4) and Eq. (5) have been processed for 3 runs with kite in static flight. Results are presented in Table IV. No kite setting was modified during or between periods, which means the global lengths of back tethers were maintained constant (no change in global angle of incidence of the kite). Only differential variations of tether lengths were done for control purpose, and to keep the kite on a static defined position.

Table IV: Compiled results of four periods with kite in static flight

| | Dura-tion (s) | Averaged True Wind Speed (m/s) | Averaged True Wind Angle (°)* | Lift to drag ratio L/D | | Lift coefficient $C_L$ | |
|---|---|---|---|---|---|---|---|
| | | | | Mean | Standard deviation | Mean | Standard deviation |
| Period 1 | 399 | 5.7 | 88 | 5.9 | 2.3 | 0.68 | 0.21 |
| Period 2 | 569 | 6.1 | 95 | 6.1 | 2.5 | 0.76 | 0.26 |
| Period 3 | 209 | 5.7 | 304 | 5.3 | 1.5 | 0.59 | 0.17 |
| *According to boat axis; for example 90° means cross wind, starboard tack | | | | | | | |

The instantaneous post processed signals for the lift to drag ratio and the lift coefficient, corresponding to Period 2 are plotted in Fig. 7 and Fig. 8. Results are varying a lot, but the average lift to drag ratio during the considered period is equal to 6.06, and the average lift coefficient is equal to 0.76. This seems consistent with other experimental data published, like Dadd ones [8]. Indeed, for a 3-square-meter kite with an aspect ratio of 4.9, Dadd got a lift coefficient of 0.78 and a lift to drag ratio of 6.07. To estimate drag coefficient and so lift to drag ratio of other kite with other aspect ratio, Dadd uses Prandtl formula as presented in Abbott and Von Doenhoff [11] and given in Eq. (6), assuming both kite are trimmed to produce same lift coefficient.

$$C_D' = C_D + \frac{{C_L}^2}{\pi}\left(\frac{1}{AR'} - \frac{1}{AR}\right) \quad (6)$$

Applying this method to the kite used for the present study (aspect ratio of 5.5), the expected lift to drag ratio should be 6.36.

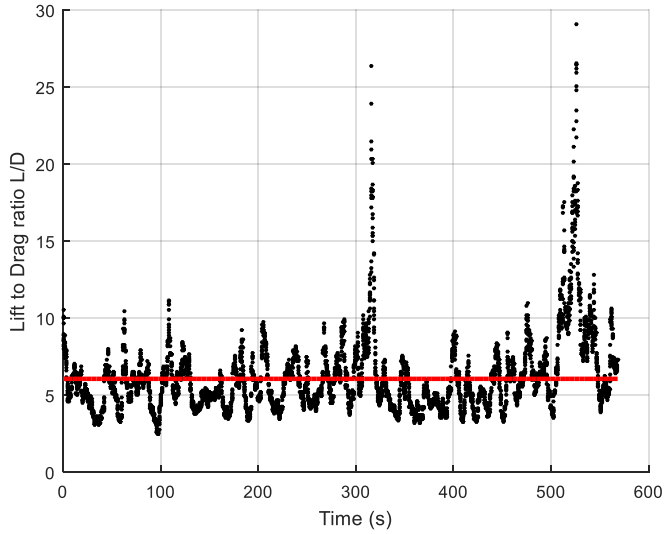


Fig. 7: Lift to drag ratio for each point using Eq. (11) (dotted), during a 569s run with kite in static flight. The solid red line is the mean of the lift to drag ratio during the considered period, and is equal to 6.06. The associated standard deviation is 2.45.

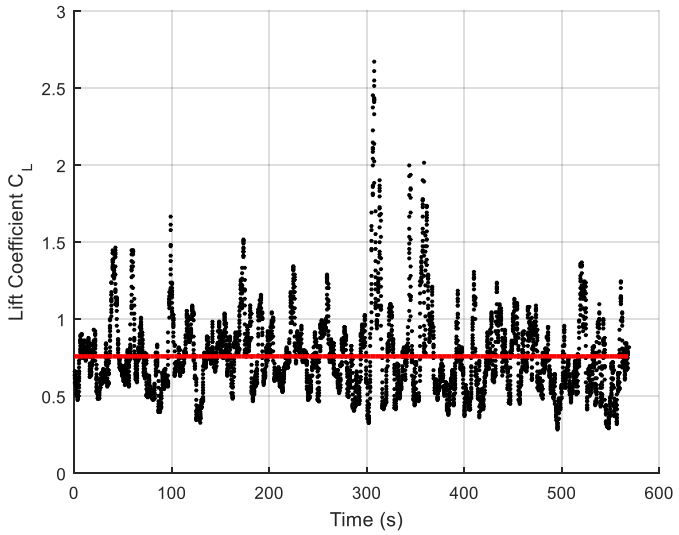


Fig. 8: Lift coefficient for each point using Eq. (12) (dotted), during a 569s run with kite in static flight. The solid line is the mean of the lift coefficient during the considered period, and is equal to 0.76. The associated standard deviation is 0.26.

## 6. Discussion

The averaged results of the 3 periods are close, with also a good agreement with published data, as it has been shown previously. However, the point to point data analysis in Fig. 7 and Fig. 8 shows extreme values of lift to drag ratio and lift coefficient that are not realistic. This demonstrates the limits of the various assumptions which have been done. One of the most important is probably the consideration of a kite velocity equal to 0 into the $\Re_{LF}$ reference frame, but the straight line assumption could also be a source of uncertainty. The decision to disregard the twist wind flow along the altitude due to a lack of data and models could be also detrimental. Indeed, a fourth period with kite in static flight has been logged, but it had to be discarded due to inconsistent data. One possible explanation is a significant difference between the wind orientation at the measurement point and the

wind orientation at the kite position. This eventuality leads us to consider, for future experimental campaign, a duplication of wind measurement systems. Moreover, the installation of multiple anemometers at various altitudes could be also a good way to improve wind estimation with altitude.

This approach has already been undertaken during another experimental campaign held in Brittany in June 2016. This campaign took place on shore, with the kite control system solidly fixed to the ground. A SOnic Detection And Ranging (SODAR) wind profiler was used to get the wind intensity and direction along altitude. The used kites were commercial ones, with area of 5-sqare-meters, and length of tethers from 25 meters to 80 meters were tested. An automatic pilot based on Fagiano work [12] was implemented to generate repeatable eight-pattern trajectories. An example of multiple eight-pattern trajectories during a ten minutes record is presented in Fig. 9. More than 15 hours of trials were logged, and data are currently under post-processing. Results will be presented and discussed in a future paper.

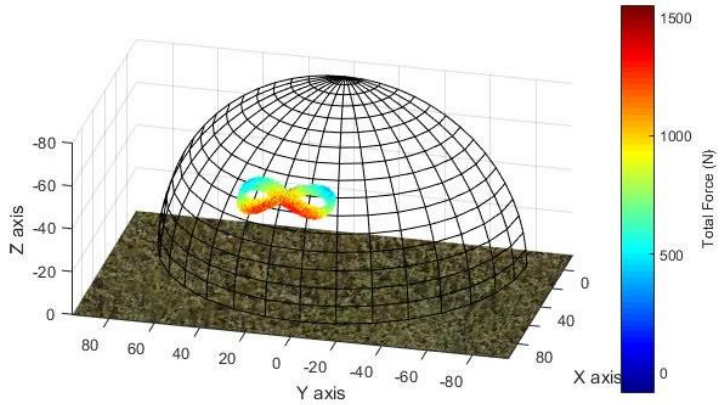


Fig. 9: Position of the kite during a ten minute record of the new experimental campaign held in Brittany in June 2016. The total force at each point is given according to the color bar.

Another goal of the on board measurement campaign was initially to benchmark the fuel savings prediction tool developed by Leloup et al. [4], using the flowmeter installed on the engine. However, due to an unexpected unavailability of the boat and unsuitable weather, it has been impossible in only one day to carry out enough measurements alternating runs with kite and then runs without kite with identical environmental conditions. Nevertheless, a first comparison can be done between power supplied by the kite, and power delivered by the engine to the propeller thanks to the sensors that were installed on-board. For example for the Period 2, on the engine side, the average rotation speed of the propeller shaft is 3.4 revolutions per second, and the average torque on the propeller shaft is 1800 Nm. The total power provided by the engine to the propeller is then 38000 W. On the kite side, the average propulsive force generated by the kite during the 569 s is 505 N, the average speed of the boat is 2.4 m/s, so the average power is 1212W. This leads to a kite providing 4.5% of the total power, with only 6.1 m/s of true wind speed, and in static flight condition. Extrapolation of this case to a true wind speed of 12m/s leads then to a kite providing 17% of the total power required. However this basic estimation needs to be treated very carefully. Indeed this is only one particular case, and it does not reflect all operational conditions of the boat. Moreover this extrapolation does not fully consider secondary effects, such as the impact of the kite on the drift of the boat. This could for instance induce bigger rudder angles in order to counteract the effects of kite, and so would affect fuel savings. The investigation of these possible issues would be done in a future work, using in particular the manoeuvrability model presented and validated by Bigi in [5]. On another hand, in the present study the kite flight tested was not optimized. Much better results should

be achieved in dynamic mode eventually.

## 7. Conclusion

A full scale kite experimental set up was installed on a13-meter fishing vessel, equipped with a 50-square-meter kite. Boat motions, engine parameters, kite forces, kite positions and wind data were recorded during one day of measurements. Multiple runs with kite in static flight were done with various durations, from 3 to 10 minutes. From data which were logged during these runs, a method for estimating lift to drag ratio and lift coefficient has been carried out. This method was computed, and showed results making sense. Thus, a lift to drag ratio about 5.9 and a lift coefficient about 0.7 could be retained (average on the 3 periods). These results are very close of those obtained by Dadd [8], even if strong assumptions have been done to get them. These assumptions have been discussed and improvements in the experimental set up for future work are under consideration.

## Acknowledgements

The authors wish to express their deep appreciation for the full support of the Steven Paul's master-owner Guy Leblanc, and his great motivation to continuously innovate. The authors are also grateful to the French agency for energy development and control (ADEME) for the funding of this study.

## References

[1] M. L. Loyd, "Crosswind Kite Power (for large-scale wind power production)," *J. Energy*, vol. 4, no. 3, pp. 106–111, 1980.

[2] L. Fagiano and M. Milanese, "Airborne wind energy: an overview," in *American Control Conference*, Montréal, 2012, pp. 3132–3143.

[3] A. Cherubini, A. Papini, R. Vertechy, and M. Fontana, "Airborne Wind Energy Systems: A review of the technologies," *Renew. Sustain. Energy Rev.*, vol. 51, pp. 1461–1476, 2015.

[4] R. Leloup, K. Roncin, M. Behrel, G. Bles, J.-B. Leroux, C. Jochum, and Y. Parlier, "A continuous and analytical modeling for kites as auxiliary propulsion devoted to merchant ships , including fuel saving estimation," *Renew. Energy*, vol. 86, pp. 483–496, 2016.

[5] N. Bigi, M. Behrel, K. Roncin, J.-B. Leroux, A. Nême, C. Jochum, and Y. Parlier, "Course keeping of ship towed by kite," in *15e Journées de l'Hydrodynamique*, Brest, 2016.

[6] "ITTC – Recommended Procedures - Full Scale Measurements Manoeuvrability Full Scale Manoeuvring Trials Procedure," in *International Towing Tank Conference*, Venice, 2002.

[7] Y. Yoshimura and Y. Masumoto, "Hydrodynamic Database and Manoeuvring Prediction Method With Medium High-Speed Merchant Ships and Fishing Vessels," *Proc. Int. MARSIM Conf.*, 2012.

[8] G. M. Dadd, "Kite Dynamics for Ship Propulsion," Ph.D. Thesis, University of Southampton, 2012.

[9] "IITTC Symbols and Terminology List," in *International Towing Tank Conference*, Copenhagen, 2014.

[10] Xsens Technologies, "MTi User Manual." 2014.

[11] I. H. Abbott and A. E. Von Doenhoff, *Theory of Wing Sections*. New York: Dover Publications Inc., 1959.

[12] L. Fagiano, A. U. Zgraggen, and M. Morari, "Automatic crosswind flight of tethered wings for airborne wind energy: modeling, control design and experimental results," *Green Energy Technol.*, pp. 167–180, 2013.